Shifting hail hazard under global warming

Timothy H. Raupach[1,2,3*], Raphael Portmann[4,5], Christian Siderius[6], Steven C. Sherwood[2,3]

[1]Institute for Climate Risk and Response, UNSW Sydney, Mathews Building Level 4, The University of New South Wales, Sydney, 2051, NSW, Australia.
[2]Climate Change Research Centre, UNSW Sydney, Australia.
[3]ARC Centre of Excellence for Climate Extremes, UNSW Sydney, Australia.
[4]Agroscope, Swiss Federal Office for Agriculture, Zurich, Switzerland (prev. address).
[5]Planval, Bern, Switzerland.
[6]Uncharted Waters, Sydney, Australia.

*Corresponding author(s). E-mail(s): timothy.h.raupach@gmail.com;

Abstract

Hailstorms cause damage across the globe, but changes to hailstorms in a warming climate are not well quantified. We applied three hail proxies to an ensemble of global model projections to quantify changes in the frequency of hail-prone conditions worldwide. Changes were divergent, with results depending on proxy treatment of temperature. Uncertainty on hail projections remains high, especially in the tropics. However, in projections with 2 °C and 3 °C of mean global warming, ensemble-mean hail-prone conditions shifted poleward, with decreases in hail hazard across the mid-latitudes and increases in colder regions. We calculated the resulting effects for 26 crop types. With fixed exposure and vulnerability, hail risk was generally projected to increase for winter crops such as wheat and decrease for summer crops such as maize. Poleward shifts in hail hazard may attenuate any positive impacts of similar shifts in crop regions under climate change.

Keywords: hail, severe weather, convection, trends, projections

Hailstorms are a form of extreme weather that causes significant damage to physical assets including crops. Hail and the storms that produce it are expected to be affected by anthropogenic global warming, yet regional studies using observations or projections show geographical inhomogeneities and there remains high uncertainty on the details of any changes [1]. Globally, hail observations are scarce [1], meaning global climatologies generally rely on satellite data [2] or examination of environmental conditions in reanalyses using hail proxies [3]. Here, we produced global projections of future hail hazard using hail proxies applied to model output from the Coupled Model Intercomparison Project (CMIP6) [4] in a per-degree framework, and used them to analyse projected changes in hail frequency and resulting changes in hail risk to crops.

Because hailstorms are hard to observe and model owing to their small spatial size and relative rarity [1], proxies that detect hail-prone atmospheric conditions are often used in climatological studies. Hail proxies rely on detecting the atmospheric "ingredients" required for hail to form. Hailstones form by accretion of supercooled liquid water onto ice embryos suspended in the updraft of a thunderstorm, until they become too heavy to support, after which they fall while melting on their descent through warmer air [5]. Hailstorm ingredients are usually considered to include, at a minimum, atmospheric instability, for a thunderstorm with strong updrafts that can support hail growth to form [6], and vertical wind shear (differences in horizontal wind by height) to "organise" the storm [7] and influence hailstone trajectories [8]. Instability–shear hail proxies are common [9]. Proxies suffer, however, from the "initiation problem", in that storms rarely initiate even in storm-prone conditions [10].

Climate change is expected to affect the ingredients for hailstorms and thus the frequency and severity of hailstorms themselves [1]. A thermodynamic expectation is of three offsetting effects: first, increased instability owing to a larger saturation deficit in a warmer atmosphere [11] leading to more storm initiation and stronger updrafts that could support larger hailstones; second, increased melting of hailstones owing to a warmer troposphere [12], thus leading to a reduction (or elimination [13]) of surface hail frequency; and third, an overall decrease in vertical wind shear [7] that is often outweighed by changes in instability [14] or may not apply locally [15]. The broad thermodynamic expectation is thus of a reduction in surface hail frequency combined with an increase in severity when hail does reach the Earth's surface [1]. However, regional studies show large geographical heterogeneity in trends in hail frequency, owing in part to offsetting in these climate change effects and in part to dynamical changes meaning that ingredient changes are not spatially uniform, while hail severity is generally expected to increase [1].

Here, we applied three globally realistic hail proxies to an ensemble of eight global projections from CMIP6, to examine projections of the frequency of hail-prone conditions globally. We used a per-degree framework [16] for simpler comparisons between models. As a sensitivity study, we investigated the effects of projected changes on hail-prone proportions of time-invariant crop growing seasons for 26 different crops. For details of the simulations and proxies used, refer to "Online methods" and the supplementary information. Our work shows that, generally, hailstorm frequency is projected to shift poleward, with decreases in warmer environments but increases in cooler

environments in future, driven primarily by changes in convective instability. Our sensitivity analysis shows that the projected changes would increase hail occurrence risk to winter crops, while decreasing occurrence risk for summer crops.

Results

Comparison to ERA5 for the historical period

Figure 1 shows a comparison between the multimodel, multi-proxy mean of annual hail-prone days for the CMIP6 models, and the multi-proxy mean of annual hail-prone days for the ERA5 reanalysis, for 1980–1999. While individual CMIP6 models produced a wide range of absolute values of hail-prone days (Supplementary Figure 1), the locations of hail hotspots agreed well between reanalysis and models. The models MPI-ESM1-2-HR and EC-Earth produced similar numbers of hail-prone days to ERA5, while MIROC6, CMCC-CM2-SR5, and CMCC-ESM2 showed moderately more and CNRM-CM6-1 and GISS-E2-1-G showed significantly more hail-prone days than ERA5. Different proxies highlighted similar geographical regions but differed in magnitudes of hail-prone days, with the Significant Hail Parameter (SHIP) [17] producing the fewest, and the Eccel proxy [18] producing the greatest number of hail-prone days, respectively. Given the models produced geographical agreement but differences in absolute numbers of hail-prone days, we focus on changes in multi-proxy, multimodel means in the rest of our analyses.

Case studies of hail-prone day anomalies

Monthly multi-proxy mean anomalies in hail-prone days derived using ERA5 reanalysis showed higher values for months with known occurrences of damaging hailstorms. The proxies produced higher than climatological average numbers of hail-prone days for February and March 2015 in northern and central India (Supplementary Figure 2), regions that were affected by hailstorms that caused major losses to wheat crops in this period [19, 20]. Similarly, the proxies highlighted areas of central and southern Europe as particularly hail-prone in June 2022 (Supplementary Figure 3), when the passage of two low-pressure systems caused high-loss hailstorm outbreaks across these regions [21]. The proxies also identified April 2015 and October 2022 as unusually hail-prone months in northeast India and western France, respectively; there were hailstorms reported in both regions during these respective months [19, 21]. These case-study results increase our confidence in the ability of the multi-proxy mean to identify hail-prone conditions worldwide, despite the individual proxies having been trained using data from Australia [9], Italy [18], and the United States [17].

Changes in hail-prone days with warming

Figure 2 shows multimodel, multi-proxy mean changes in annual hail-prone days for 2 °C and 3 °C of global warming, respectively. These changes are shown as relative differences zoomed to selected land areas in Figure 3. Changes were similar between the two epochs, with a general increase in the change magnitude in the 3 °C scenario. Changes generally agreed in sign across the Raupach proxy and SHIP, while the pure

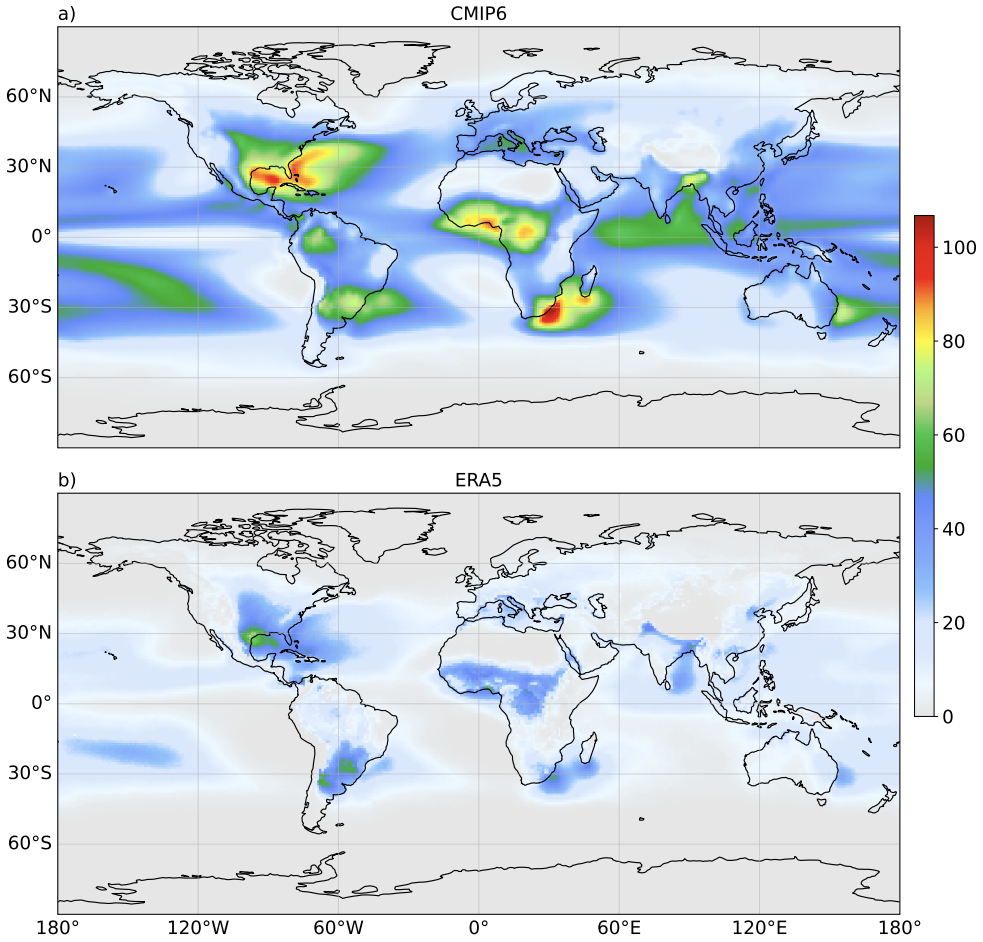

Fig. 1 Hail proxies show known hail-prone regions in both global models and reanalysis. Multimodel, multi-proxy mean annual hail-prone days for CMIP6 models (a), and multi-proxy mean annual hail-prone days for ERA5 reanalysis (b), for three selected proxies over the historical period (1980-1999) at 1 × 1 ° resolution.

instability–shear proxy of Eccel [18] produced contrasting increases across the tropics (Supplementary Figure 4) that lead to high uncertainty in the tropics, especially in Asia and the Americas. The mean changes show an overall poleward shift of hail-prone conditions under both warming scenarios, with increases in hail-prone conditions frequency projected across land areas in central-north Asia, New Zealand, the southeast of Australia, North America north of about 50° N, South America in the southern Pampas and west to the Andes, and Europe north of about 60° N, in the vicinity of the Alps, and southeast of the Black Sea. Decreases in hail-prone day frequency were projected in southeast coastal areas of India and China, connecting in a band across mainland Southeast Asia, northern Australia, the southeast United States and Mexico, southeast South America east of the Andes between about 15° S and 30° S, and

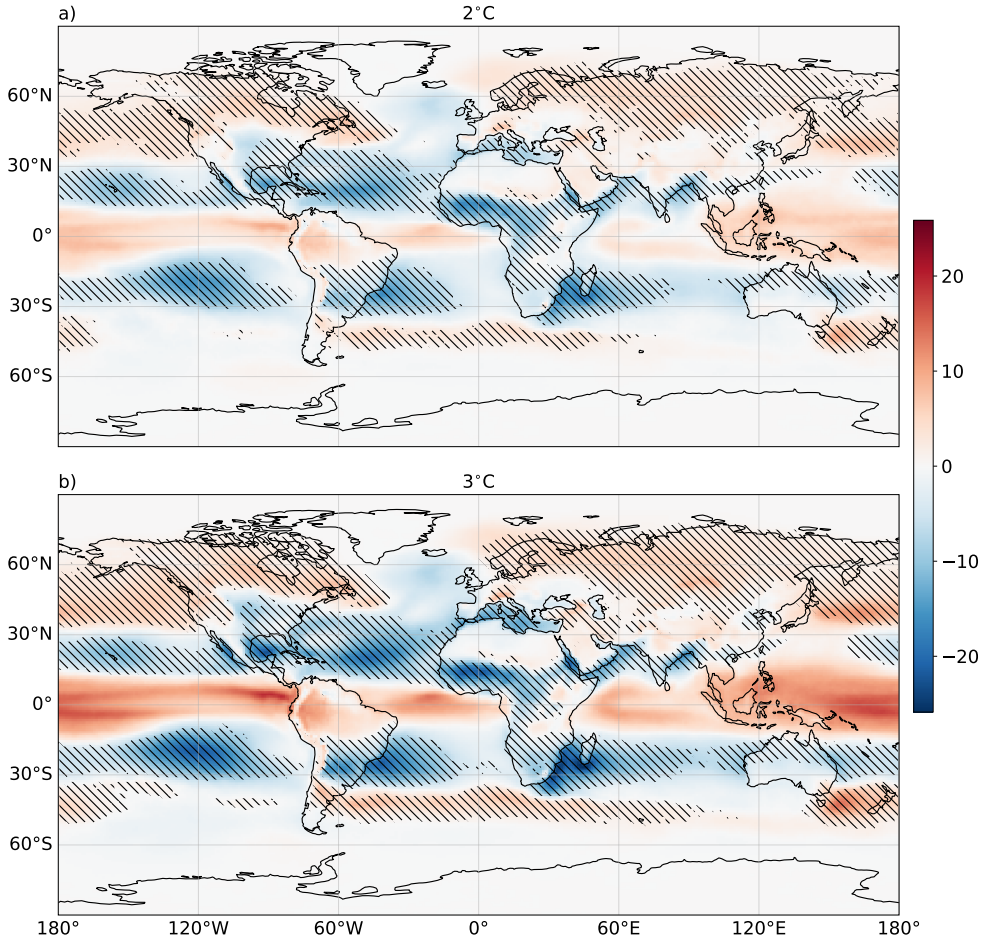

Fig. 2 Hail-prone conditions shift under warming projections. Multi-proxy, multimodel mean changes in annual hail-prone days for 2 °C (a) and 3 °C (b) of global warming. Stippling shows regions in which at least 50% of the model/proxy combinations agreed with the sign of the mean difference and also showed significant differences in the mean ($p < 0.05$ on a t-test on two related samples).

most of Africa south of 15° N. Changes by season are shown in Figure 4, and show that the increases (decreases) shift poleward in the cold (warm) season.

Projected changes in proxy ingredients

Projections of storm-relevant properties showed almost uniform increases in convective instability, with increases in extreme values of convective available potential energy (CAPE) and lifted index (LI), and increasing convective inhibition that may lead to more explosive development of severe storms (Supplementary Figure 5). Projections in extremes in 0-6 km bulk wind shear (S06) showed decreases (mixed increases) in

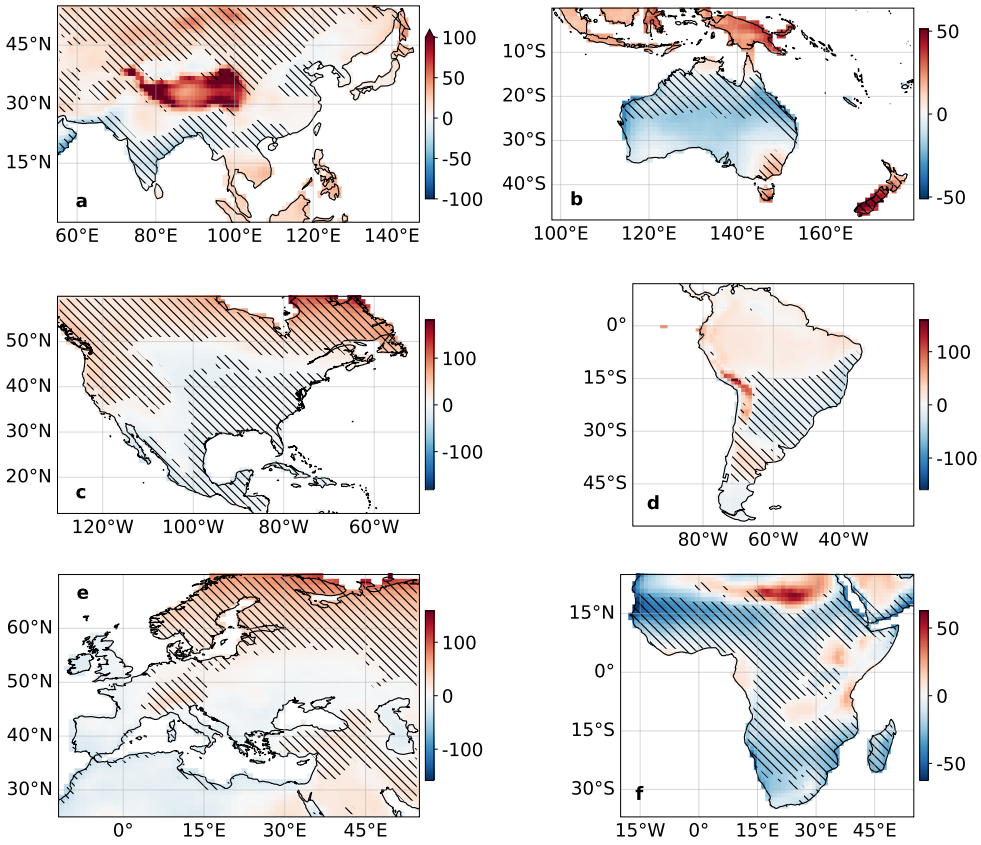

Fig. 3 Multi-proxy, multimodel mean changes in annual hail-prone days by region. Changes are shown as a percentage of multi-proxy, multimodel mean historical hail-prone days over land, for 2°C warming (a-c) and 3°C warming (g-i) for Asia (a, g), Australasia (b, h), and North America (c, i). Stippling as for Figure 2. Colour bars are shared across rows; to increase contrast the colour bar for a is truncated.

the northern (southern) hemisphere (Supplementary Figure 5). Temperature-related ingredients increased as expected in the warmer scenarios (Supplementary Figure 6).

Drivers of the projected changes

Figure 5 shows the main drivers of projected changes in this study, shown as the difference between projected changes and changes when the future values for single ingredients were de-biased. The ingredients driving the changes depended on the proxy. Overall, increases in hail-prone environment frequency were driven by instability increases, while reductions in hail-prone environment frequency were driven by temperature-related ingredients. The sums of changes across de-biased ingredients were close to the projected changes where no ingredients were de-biased, indicating that these results explain most of the projected changes, with the small differences that remain likely related to interactions between ingredients. The large differences

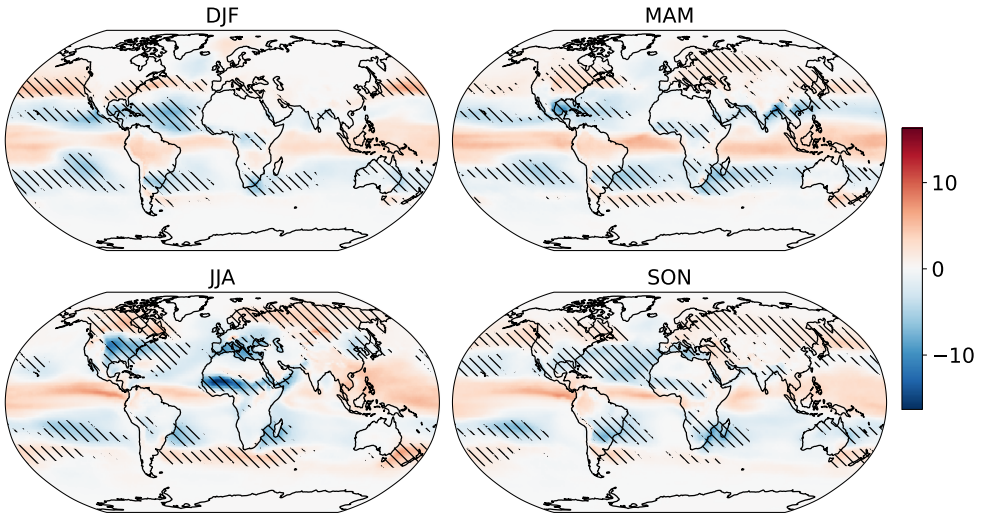

Fig. 4 Multimodel, multi-proxy mean differences in hail-prone days by season for 3 °C global warming. DJF stands for December, January, February; MAM stands for March, April, May; JJA stands for June, July, August; SON stands for September, October, November. Stippling as for Figure 2.

between the Eccel proxy and the other proxies were caused by the instability–shear proxy reacting to increases in instability without explicitly accounting for temperature changes. Changes in SHIP were driven mainly by changes in the most-unstable mixing ratio. In the Raupach proxy, increases in hail-prone days owing to instability increases are offset by changes in melting level height and T_{500}.

Changes in hail-prone proportions of cropping periods

Figure 6 shows changes in the proportion of crop growing time considered hail-prone, for 26 crops by world region. We use a new metric, the hail-prone proportion of cropping season (HPP, the proportion of total cropping days considered hail prone) to measure relative hail occurrence hazard per crop for a given location. For the historic period, the African tropics showed particularly high hail hazard for sorghum, millet, groundnuts/peanuts, rice, soybeans, maize, and pulses (Supplementary Figure 7). Warming of 2°C and 3°C C was projected to reduce HPP for these crops while increasing HPP for crops grown in more poleward regions (Supplementary Figure 8).

In Africa, all crops were projected to experience fewer hail-prone days, with regional increases not statistically significant (Supplementary Figure 9). In Asia, (Supplementary Figure 10), there were a range of responses for most crops, with decreasing hail hazard in India and southeastern in China, but increases in HPP across the north. Maize was projected to experience a greater hail hazard in southeastern China but a lesser hazard in the northeast, while wheat and rapeseed/canola showed strong increases in HPP in northeastern China. In Europe, most significant changes were increases, with projected increases in HPP for barley, fodder grasses, grapes/vine,

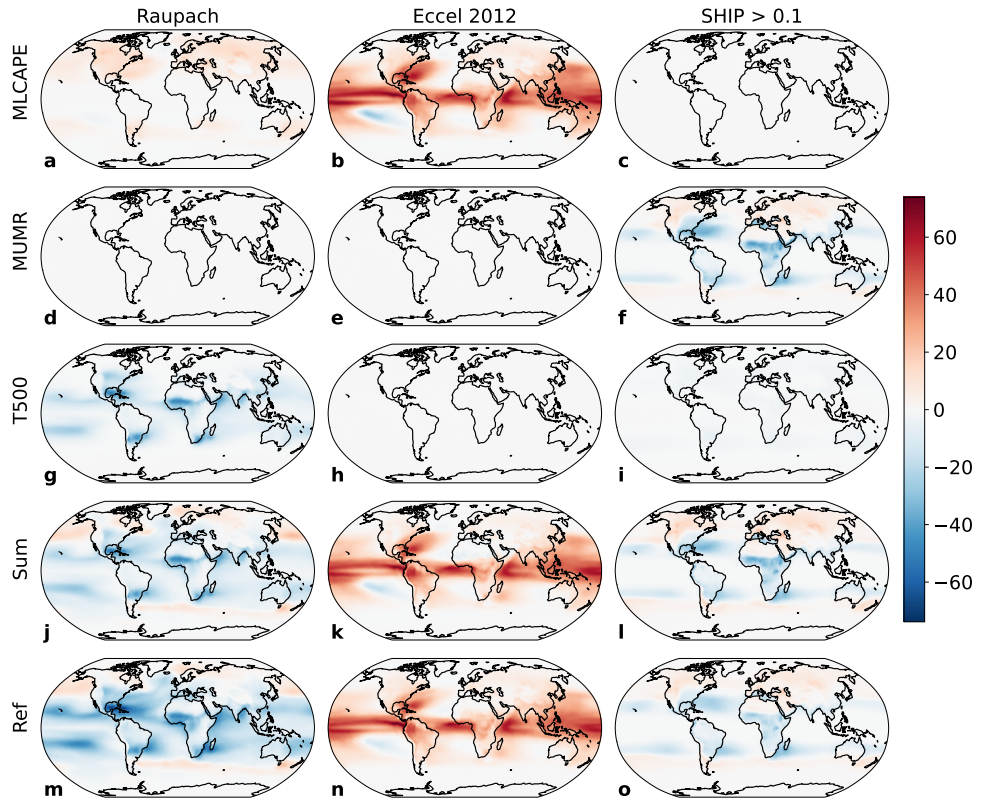

Fig. 5 The main drivers of the projected changes. All drivers are shown in Supplementary Figure 22. All plots are multimodel means. Plots show the difference in hail prone days between historical and the 3C epoch for unchanged ingredients, minus the difference with the given ingredient de-biased in the 3C epoch. Red (blue) areas show where an ingredient added to (subtracted from) the projected change. Ingredients shown here are melting level height (MLH, a-d), mixed-layer CAPE (MLCAPE, e-h), most-unstable mixing ratio (MUMR, i-l), and temperature at 500 hPa (T500, m-p). "Sum" (q-t) shows sums across changes from all de-biased ingredients (column sums from Supplementary Figure 22) and "Ref" (u-x) shows the projected changes per proxy when no ingredients were de-biased. Columns show hail proxies and the colour scale is in annual hail days.

maize, potatoes, pulses, rapeseed/canola, rye, wheat, and other annual and perennial crops. The significant increases were generally concentrated in a zonal band at around 60°N and in regions around the Alps in Western Europe, an area to the southeast of the Black Sea, and in southern Iran (Supplementary Figure 11). Increases in HPP for rye were heavily concentrated in Finland, Estonia, Latvia, and the adjoining areas of Russia. In North America, there were significant increases for barley and rye in particular, with regional increases in HPP for these crops across the central and eastern USA. For other crops, there were generally decreases in HPP projected in the southeast, with increases projected in the northwest and across northern Canada (Supplementary Figure 12). In Oceania overall, barley was projected to have increased hail hazard, albeit with a large range in projected changes, while all other crops showed

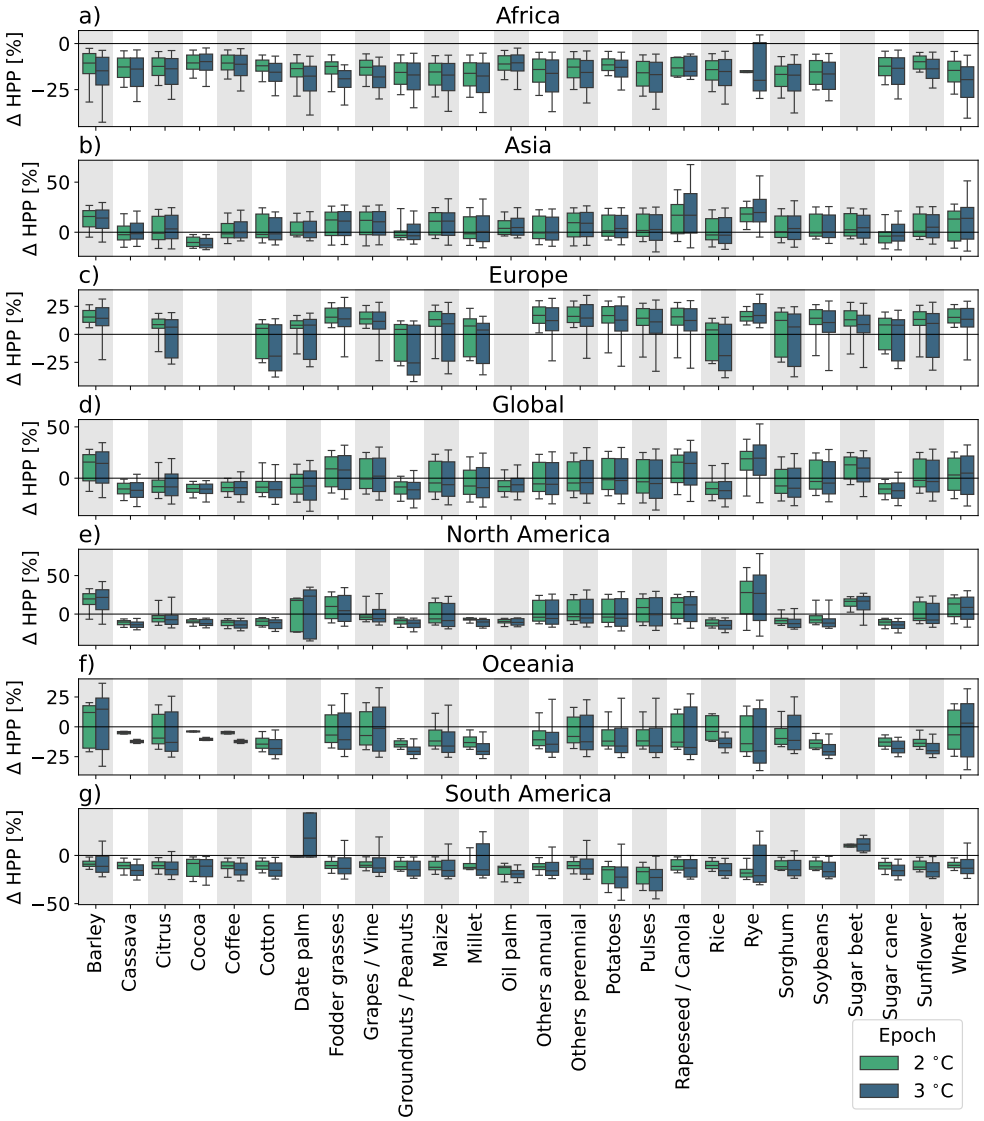

Fig. 6 Distributions of significant changes in hail-prone crop proportion (HPP) by crop, epoch, and world region. Regions are defined as in Figure 3. Changes are multimodel, multi-proxy mean changes in hail-prone proportion of cropping season (HPP), shown as a percentage of the multimodel, multi-proxy mean historical HPP. Significant changes are those for which at least 50% of the model/proxy combinations agreed with the sign of the mean difference and also showed significant differences in the mean ($p < 0.05$ using Welch's t-test). Coloured boxes show interquartile ranges, whiskers show 10th-90th percentile ranges.

projected decreases in HPP. Significant decreases in HPP were concentrated in Australia's northeast, while significant increases were concentrated in a small region of southeast Australia and the South Island of New Zealand (Supplementary Figure 13).

In South America, all crops were projected to have decreased overall hazard, except date palm and sugar beet which both have small growing areas. However, regional changes show statistically significant increases in HPP for several crops, for example maize and potatoes, in a region of the southern Pampas and west to the Andes (Supplementary Figure 14).

Monthly changes for point locations (Supplementary Figures 15–21) highlight that the crops with the greatest projected increases in risk were those with winter cropping periods, while those with the greatest reductions in risk were those that grow across summer periods. For example, in China, potatoes were projected to have decreased risk during the cropping season of May to September, while wheat was projected to have increased risk during its season from October to April (Supplementary Figure 16). These plots also show that uncertainty was higher for the summer months, with greater inter-model spread and with the sign of the change disagreeing between proxies for some months. Returning to the two case studies shown earlier, a region of southern Europe near the Alps showed an overall increase in hail-prone proportion of cropping season for potatoes, rye, and wheat, with proxy disagreement across the summer months and agreement on increases from October to April (Supplementary Figure 19). In India for rice, wheat and maize, there were non-significant increases in cropping season hail-prone proportion across the southern flank of the Himalaya, but decreases further south (Supplementary Figure 21).

Discussion

We applied three hail proxies to an ensemble of eight global projections. The proxy results were divergent, with the Raupach and SHIP proxies that take temperature explicitly into account projecting decreases in hail-prone condition frequency across the tropics, while the instability–shear proxy of Eccel projected strong increases in these regions. This inconsistency is explained by temperature changes: the Raupach proxy, in particular, has a strong feature interaction where the height of the melting level affects the relative importance of instability versus shear in the proxy [9] (see also Supplementary Material Section 2). The analysis of drivers (Figure 5) shows this interaction, with the Raupach proxy less sensitive to instability in the tropics than in the mid-latitudes. Instability–shear proxies have a tendency to overestimate hail probability in the tropics, [9], which motivated development of the Raupach proxy. The disagreement between proxy projections means there remains high uncertainty on projections on hail hazard changes, particularly in the tropics.

Our projections show broad poleward shifts in ensemble-mean hail-prone condition occurrence frequency under 2 °C and 3 °C of warming, with, generally, decreases in summer hail-prone day frequency and smaller increases in winter. The increases are driven by changes in instability and offset by increases in temperature. A sensitivity analysis on 26 crop types shows that winter crops are most susceptible to increases in hail hazard while summer crops are most likely to experience a reduction in hail hazard. It is interesting to compare our results to those for the broader class of severe convective storms, which includes thunderstorms that do not produce hail. Severe storm conditions are generally projected to increase in frequency with global warming

[16]. Similar to the differences between the Eccel and Raupach/SHIP proxies discussed above, our results indicate that changes in hail conditions may differ from those in overall storm conditions because of temperature changes – that is, increasing hailstone melt in warmer conditions, which is especially important for smaller hail [13].

To put our global analysis of changes in hail hazard frequency under climate change in context, here we show where our projections agree with or contradict previous results [1], by region. In Asia, our results match past decreases in hail occurrence found in stations concentrated in China's east from 1980-2012 [22], but contradict past decreases in hail events reported in Mongolia (1993-2013) [23]. In Australia, our significant projections continue observed trends: hail-prone conditions in reanalysis (1979-2021) have increased in the southeast and southwest of the country with decreases across the north and centre [24] (our non-significant projected decreases in frequency in the southwest contradict these past trends). Projections for small regions in the southeast have shown no trends in hail losses for doubled CO2 concentrations [25]. A decrease in frequency in point locations in southwest Victoria was projected when comparing 1980-2000 to 2040-2060 [26], although the decreases were based on decreases in instability that do not agree with more recent analyses [27].

In North America, past trends show a mixed picture [1], but our projections align with some previous results: hailstorm frequency increased in Alberta, Canada from 1982-1993 compared to 1977-1982 [28], there increases in frequency the central Rockies with overall USA decreases close to 2000 (although increases were noted in the high plains and southeast, contradicting our results) [29], and a poleward shift was found in hail reports since 2000 in the Eastern United States [30]. Regional projections for North America comparing 1971-2000 to 2041-2070 have shown decreases in frequency overall and especially in the east and southeast [31] and a near elimination of surface hail in Colorado [13], agreeing with our projections. Severe hail frequency in North America is generally projected to increase [32], although summer decreases in severe hail frequency in the east are projected [32]. In South America, there are few trend studies and no other projections [1]; in Argentina our significant projections contradict observed decreases in the centre and east over 1960-2008, although there is geographical variability in observed trends in Argentina [33].

In Europe, our results showed significant projected increases to the north of the Alps, agreeing with past increases in Switzerland in insurance data (1949-1993) [34], Switzerland (1959-2022) [35] in reanalyses, and Southern Germany (1986-2004) in insurance records [36]. Much of the rest of southern and central Europe showed non-significant changes in our analysis, which aligns with the wide variety of observed trends and corresponding high uncertainty for both trends and projections in this region [1]. In Germany, where our results were non-significant, regional projections to 2050 have shown increases in hail-related weather types [37] and an increase in hail potential in the northwest and south [38]. Likewise in central Italy our results were non-significant while a previous regional projection to 2040 showed an increase in annual hail frequency [39]. Increased melting in Atlantic France is projected to reduce hailstone numbers [40]. Severe hail frequency in Europe is generally projected to increase by 2100 [15] with model disagreement on instability trends over the United Kingdom [41].

In our work we have used CMIP6 projections that include changes in atmospheric circulations, thus avoiding a purely thermodynamic approach. However, we note that there is generally low confidence in how changes in dynamics affect extreme events [42], and for the broader class of severe convective storms changes in reanalysis periods [43] can be of different sign to projected changes [16], which may be partly explained by uncertainty introduced by changes in atmospheric circulation. Proxies trained in one region cannot be assumed to be perfectly applicable globally since storm properties differ by location [6, 9]. However, the Raupach proxy is specifically designed to take spatial variability in storm conditions into account by using the melting level height, and have been shown to perform reasonably across the Australian continent which contains a wide variety of storm environments [24], and the multi-proxy means were able to identify particularly hail-prone conditions in case studies in areas in which the proxies used here were not trained. Although we show proxy results globally, we note the proxies used were trained using land-based reports [9, 18] and there is uncertainty in the occurrence of hail in maritime storms [5].

Our results showing the effects of the projected changes on hail-prone cropping periods contribute to understanding climate impacts on global food production. Most previous studies have concentrated on temperature, precipitation, and CO2 changes, and neglect infrequent but high-impact extreme weather such as hailstorms [44]. A limitation to our approach is that the cropping periods we consider are stationary in time and relatively coarse, so our analysis of crop changes should be taken as a sensitivity study rather than projections of changes in crop damage or yield. Suitable growing regions and cropping periods may also shift poleward with warming [45] with some positive impacts on yields [44]. Our study shows that similar shifts in hail hazard may attenuate any positive impact on crop yields in a warming world. For maize, an important staple grown in tropical regions, a potential reduction in hail hazard would only lessen the projected severe reduction in yield owing to increasing temperatures [44]. It is also important to note that the timing of hail events within the broad cropping season strongly influences possible crop damage [46]. Future analyses should take projected changes in cropping season and growth stages into account.

Our results show large areas of projected reductions in hail-prone day frequency. However, given proxy limitations, we do not examine changes in hailstorm severity or hailstone size. Projected increases in atmospheric instability (Supplementary Figure 5) in regions in which sufficient moisture is available would generally be expected to increase generation of large hailstones that could survive melting to the surface [1], meaning that even where frequency is projected to reduce, severity may increase. A coincident decrease of small hail and increase of large hail aligns with hail size end-of-century projections for the USA [47]. It is likely that global severe hail projections would differ significantly from the "any hail" projections shown here.

Online methods

Data

A filtering approach was used to select models from the Coupled Model Intercomparison Project Phase 6 (CMIP6) [4]. We selected models that contained variables

required to calculate convective indices: air temperature at the surface (`tas`) and by model level (`ta`), wind vectors at the surface (`uas` and `vas`) and by level (`ua` and `va`), specific humidity at the surface (`huss`) and by level (`hus`), and surface pressure (`ps`). We filtered for models with a temporal resolution at least as fine as six-hourly (those with "table IDs" of `3hr` or `6hrLev`), and models that were available for both historical and SSP5-8.5 experiments ("experiment IDs" of `historical` or `ssp585`). Further, the models had to be available in the National Computational Infrastructure (NCI) node of the Earth System Grid Federation (ESGF), and had to cover the required epochs. The resulting CMIP6 models, that we used here, are detailed in Supplementary Table 1. If model orography was available in the `orog` variable, it was used; if not, the orography of the historical runs of CNRM-CM6-1 (ensemble r1i1p1f2) was interpolated onto the model grid and used instead [48]. Reanalyses were European Centre for Medium-range Weather Forecasts (ECMWF) reanalysis 5 (ERA5) data [49] on pressure levels. To match the CMIP6 model characteristics, we used global ERA5 data at 00, 06, 12, and 18 UTC for each day from 1980 to 1999, interpolated to $1° \times 1°$ resolution.

Calculation of convective parameters

Convective parameters were calculated as described for the proxy of Raupach et al., 2023 [9], for each CMIP6 dataset at its native resolution and for downscaled ERA5 data. For each CMIP6 model, annual and seasonal statistics were calculated, then all statistics were interpolated onto a $1° \times 1°$ grid for comparison.

Application of hail proxies

We applied three hail-specific instability-shear proxies to CMIP6 and ERA5 data: Raupach, Eccel, and SHIP. The proxies were, respectively, a modified version of the proxy in Raupach et al., 2023 with "extra conditions" to remove false positives (Raupach) [9], that of Eccel et al., 2012 [18], and a threshold of 0.1 on the Significant Hail Parameter (SHIP) [17]. The modifications made to the Raupach proxy are detailed in Supplementary Material Section 2. Other proxies were tested but excluded from this study because they produced unrealistically many or too few hail-prone days in comparison with the other proxies (Supplementary Figure 23). The Raupach proxy without extra conditions produced similar results to the Raupach proxy with extra conditions (Supplementary Figure 23 **(and changes)**).

Per-degree framework

The historical period used for each model was 1980–1999. The epochs that represented 2 °C and 3 °C warming compared to the historical period were determined per model using 20-year running means of monthly global average temperature anomalies (Supplementary Figure 24).

Calculation of drivers

For each hail proxy ingredient, de-biased versions of the 3 °C epoch were calculated using `python-cmethods` [50] using the quantile-mapping method with 100 quantiles and the historical period as the baseline.

Data availability. MIRCA2000 data are available with identifier https://doi.org/10.5281/zenodo.7422506. ERA5 data are available with identifier https://doi.org/10.24381/cds.bd0915c6. CMIP6 data are available with identifier https://doi.org/10.25914/Q1CT-RM13.

Code availability. Convective indices were calculated using `xarray_parcel` by T. H. Raupach (https://doi.org/10.5281/zenodo.15081094). Warming levels were calculated using code by T. H. Raupach (https://doi.org/10.5281/zenodo.10785698). De-baising code was `python-cmethods` by B. T. Schwertfeger (https://doi.org/10.5281/zenodo.12168002).

Acknowledgements. This research was undertaken with the assistance of resources and services from the NCI, which is supported by the Australian Government. THR acknowledges financial support from QBE Insurance.

Competing interests. Since March 2024 THR's position at UNSW Sydney has been financially supported by QBE Insurance. The authors declare no other competing financial or non-financial interests.

Author contributions. THR designed the study, performed the analyses, wrote the manuscript, and created the figures. RP suggested the crop analysis. RP, CS, and SCS contributed to interpretation of results, design of analyses, and editing of the paper.

References

[1] Raupach, T. H. *et al.* The effects of climate change on hailstorms. *Nat. Rev. Earth Environ.* **2**, 213–226 (2021).

[2] Bang, S. D. & Cecil, D. J. Constructing a multifrequency passive microwave hail retrieval and climatology in the GPM domain. *J. Appl. Meteorol.* **58**, 1889–1904 (2019).

[3] Prein, A. F. & Holland, G. J. Global estimates of damaging hail hazard. *Weather Clim. Extremes* **22**, 10–23 (2018).

[4] Eyring, V. *et al.* Overview of the Coupled Model Intercomparison Project Phase 6 (CMIP6) experimental design and organization. *Geosci. Model Dev.* **9**, 1937–1958 (2016).

[5] Knight, C. A. & Knight, N. C. in *Hailstorms* (ed.Doswell, C. A.) *Severe Convective Storms* 223–254 (American Meteorological Society, Boston, MA, 2001).

[6] Brooks, H. E., Lee, J. W. & Craven, J. P. The spatial distribution of severe thunderstorm and tornado environments from global reanalysis data. *Atmos. Res.* **67-68**, 73–94 (2003). European Conference on Severe Storms 2002.

[7] Brooks, H. E. Severe thunderstorms and climate change. *Atmos. Res.* **123**, 129–138 (2013).

[8] Lin, Y. & Kumjian, M. R. Influences of CAPE on hail production in simulated supercell storms. *J. Atmos. Sci.* **79**, 179–204 (2022).

[9] Raupach, T. H., Soderholm, J., Protat, A. & Sherwood, S. C. An improved instability–shear hail proxy for australia. *Mon. Weather Rev.* **151**, 545–567 (2023).

[10] Tippett, M. K., Allen, J. T., Gensini, V. A. & Brooks, H. E. Climate and hazardous convective weather. *Curr. Clim. Change Rep.* **1**, 60–73 (2015).

[11] Seeley, J. T. & Romps, D. M. Why does tropical convective available potential energy (CAPE) increase with warming? *Geophys. Res. Lett.* **42**, 10,429–10,437 (2015).

[12] Prein, A. F. & Heymsfield, A. J. Increased melting level height impacts surface precipitation phase and intensity. *Nat. Clim. Change* **10**, 771–776 (2020).

[13] Mahoney, K., Alexander, M. A., Thompson, G., Barsugli, J. J. & Scott, J. D. Changes in hail and flood risk in high-resolution simulations over Colorado's mountains. *Nat. Clim. Change* **2**, 125–131 (2012).

[14] Trapp, R. J., Diffenbaugh, N. S. & Gluhovsky, A. Transient response of severe thunderstorm forcing to elevated greenhouse gas concentrations. *Geophys. Res. Lett.* **36**, L01703 (2009).

[15] Rädler, A. T., Groenemeijer, P. H., Faust, E., Sausen, R. & Púčik, T. Frequency of severe thunderstorms across Europe expected to increase in the 21st century due to rising instability. *npj Clim. Atmos. Sci.* **2**, 30 (2019).

[16] Lepore, C., Abernathey, R., Henderson, N., Allen, J. T. & Tippett, M. K. Future global convective environments in CMIP6 models. *Earth's Future* **9**, e2021EF002277 (2021).

[17] NOAA SPC. Significant hail parameter. https://www.spc.noaa.gov/exper/mesoanalysis/help/help_sigh.html (2022). National Oceanographic and Atmospheric Administration National Weather Service Storm Prediction Center, accessed 21 June 2022.

[18] Eccel, E., Cau, P., Riemann-Campe, K. & Biasioli, F. Quantitative hail monitoring in an alpine area: 35-year climatology and links with atmospheric variables.

Int. J. Climatol. **3**, 503–517 (2012).

[19] Chattopadhyay, N., Devi, S. S., John, G. & Choudhari, V. Occurrence of hail storms and strategies to minimize its effect on crops. *Mausam* **68**, 75–92 (2017).

[20] Singh, S. K., Saxena, R., Porwal, A., Ray, N. & Ray, S. S. Assessment of hailstorm damage in wheat crop using remote sensing. *Curr Sci India* **112**, 2095–2100 (2017).

[21] Pucik, T. Major hailstorms of 2022 (2023). URL https://www.essl.org/cms/major-hailstorms-of-2022/. Accessed 2024-01-10.

[22] Li, M., Zhang, Q. & Zhang, F. Hail day frequency trends and associated atmospheric circulation patterns over China during 1960-2012. *J. Climate* **29**, 7027–7044 (2016).

[23] Lkhamjav, J., Jin, H.-G., Lee, H. & Baik, J.-J. A hail climatology in mongolia. *Asia-Pacific Journal of Atmospheric Sciences* **53**, 501–509 (2017).

[24] Raupach, T. H., Soderholm, J. S., Warren, R. A. & Sherwood, S. C. Changes in hail hazard across australia: 1979-2021. *npj Clim. Atmos. Sci.* **6**, 143 (2023).

[25] McMaster, H. J. The potential impact of global warming on hail losses to winter cereal crops in New South Wales. *Clim. Change* **43**, 455–476 (1999).

[26] Niall, S. & Walsh, K. The impact of climate change on hailstorms in southeastern Australia. *Int. J. Climatol.* **25**, 1933–1952 (2005).

[27] Allen, J. T., Karoly, D. J. & Walsh, K. J. Future australian severe thunderstorm environments. part i: A novel evaluation and climatology of convective parameters from two climate models for the late twentieth century. *J. Climate* **27**, 3827–3847 (2014).

[28] Etkin, D. & Brun, S. E. A note on Cnada's hail climatology: 1977-1993. *Int. J. Climatol.* **19**, 1357–1373 (1999).

[29] Changnon, S. A. & Changnon, D. Long-term fluctuations in hail incidences in the United States. *J. Climate* **13**, 658–664 (2000).

[30] Liu, J. *et al.* Observed northward shift of large hailstorms in the eastern United States since 2000. *Environ. Res. Lett.* **19**, 024010 (2024).

[31] Brimelow, J. C., Burrows, W. R. & Hanesiak, J. M. The changing hail threat over North America in response to anthropogenic climate change. *Nat. Clim. Change* **7**, 516–523 (2017).

[32] Trapp, R. J., Hoogewind, K. A. & Lasher-Trapp, S. Future changes in hail occurrence in the United States determined through convection-permitting dynamical

downscaling. *Journal of Climate* **32**, 5493–5509 (2019).

[33] Mezher, R. N., Doyle, M. & Barros, V. Climatology of hail in Argentina. *Atmospheric Research* **114-115**, 70–82 (2012).

[34] Willemse, S. *A statistical analysis and climatological interpretation of hailstorms in Switzerland*. Doctoral thesis (1995). URL https://www.research-collection.ethz.ch/handle/20.500.11850/142192.

[35] Wilhelm, L., Schwierz, C., Schröer, K., Taszarek, M. & Martius, O. Reconstructing hail days in Switzerland with statistical models (1959–2022). *Natural Hazards and Earth System Sciences* **24**, 3869–3894 (2024).

[36] Kunz, M., Sander, J. & Kottmeier, C. Recent trends of thunderstorm and hailstorm frequency and their relation to atmospheric characteristics in southwest Germany. *Int. J. Climatol.* **29**, 2283–2297 (2009).

[37] Kapsch, M. L., Kunz, M., Vitolo, R. & Economou, T. Long-term trends of hail-related weather types in an ensemble of regional climate models using a Bayesian approach. *J. Geophys. Res.-Atmos.* **117**, D15107 (2012).

[38] Mohr, S., Kunz, M. & Keuler, K. Development and application of a logistic model to estimate the past and future hail potential in Germany. *J. Geophys. Res.-Atmos.* **120**, 3939–3956 (2015).

[39] Piani, F., Crisci, A., De Chiara, G., Maracchi, G. & Meneguzzo, F. Recent trends and climatic perspectives of hailstorms frequency and intensity in Tuscany and Central Italy. *Nat. Hazards Earth Sys.* **5**, 217–224 (2005).

[40] Dessens, J., Berthet, C. & Sanchez, J. L. Change in hailstone size distributions with an increase in the melting level height. *Atmos. Res.* **158-159**, 245–253 (2015).

[41] Sanderson, M. G. *et al.* Projected changes in hailstorms during the 21st century over the UK. *Int. J. Climatol.* **35**, 15–24 (2015).

[42] Seneviratne, S. *et al.* in *Weather and climate extreme events in a changing climate* (eds Masson-Delmotte, V. *et al.*) *Climate Change 2021: The Physical Science Basis. Contribution of Working Group I to the Sixth Assessment Report of the Intergovernmental Panel on Climate Change* book section 11, 1513–1765 (Cambridge University Press, Cambridge, UK and New York, NY, USA, 2021). URL https://www.ipcc.ch/report/ar6/wg1/downloads/report/IPCC_AR6_WGI_Chapter11.pdf.

[43] Taszarek, M., Allen, J. T., Marchio, M. & Brooks, H. E. Global climatology and trends in convective environments from ERA5 and rawinsonde data. *npj Clim. Atmos. Sci.* **4**, 35 (2021).

[44] Jägermeyr, J. *et al.* Climate impacts on global agriculture emerge earlier in new generation of climate and crop models. *Nat. Food* **2**, 873–885 (2021).

[45] Franke, J. A. *et al.* Agricultural breadbaskets shift poleward given adaptive farmer behavior under climate change. *Glob. Change Biol.* **28**, 167–181 (2022).

[46] Dhillon, G. S. *et al.* Effects of simulated hail damage and foliar-applied recovery treatments on growth and grain yield of wheat, field pea, and dry bean crops. *Can. J. Plant Sci.* **101**, 758–769 (2021).

[47] Gensini, V. A. *et al.* Hailstone size dichotomy in a warming climate. *npj Clim. Atmos. Sci.* **7**, 185 (2024).

[48] Bracegirdle, T. J. *et al.* Twenty first century changes in Antarctic and Southern Ocean surface climate in CMIP6. *Atmos. Sci. Lett.* **21**, e984 (2020).

[49] Hersbach, H. *et al.* The ERA5 global reanalysis. *Q. J. Roy. Meteor. Soc.* **146**, 1999–2049 (2020).

[50] Schwertfeger, B. T. btschwertfeger/python-cmethods: v2.3.0 (2024). URL https://doi.org/10.5281/zenodo.12168002.